INTERNATIONAL ATOMIC ENERGY AGENCY
UNITED NATIONS EDUCATIONAL, SCIENTIFIC AND CULTURAL ORGANIZATION
INTERNATIONAL CENTRE FOR THEORETICAL PHYSICS
I.C.T.P., P.O. BOX 586, 34100 TRIESTE, ITALY. CABLE: CENTRATOM TRIESTE

UNITED NATIONS INDUSTRIAL DEVELOPMENT ORGANIZATION

INTERNATIONAL CENTRE FOR SCIENCE AND HIGH TECHNOLOGY
c/o INTERNATIONAL CENTRE FOR THEORETICAL PHYSICS 34100 TRIESTE (ITALY) VIA GRIGNANO, 9 (ADRIATICO PALACE) P.O. BOX 586 TELEPHONE [illegible] TELEFAX [illegible] TELEX [illegible]

SMR/548-3

Course on Oceanography of Semi-Enclosed Seas
15 April - 3 May 1991

"Waves in the Gulf of California"

M. HENDERSHOTT
Scripps Institute of Oceanography
University of California - San Diego
USA

WAVES IN THE GULF OF CALIFORNIA - M. HENDERSHOTT
Trieste, 1991

1.Tides and Tidal Dissipation in the Gulf of California

The Gulf of California may be idealized as a waveguide of, say width W and depth D. In such a waveguide Kelvin modes of the form $\zeta \approx \exp[-i\sigma t+iky-xf/c]$ or $\zeta \approx \exp[i\sigma t-iky+xf/c]$ propagate along the waveguide with dispersion relation $\sigma=kc$, where $c=\sqrt{gD}$. Poincaré modes have the form $\zeta= \cos(n\pi x/W+\text{phase factor})\exp(-i\sigma t+iky)$ with dispersion relation $\sigma^2 = f^2 + c^2(l^2+(n\pi/W)^2)$.

They are evanescent along the waveguide e.g. l is imaginary if $(\sigma^2 - f^2 - c^2(n\pi/W)^2) < 0$. This happens if the frequency is subinertial or even in the superinertial case if D is large enough or W is small enough. In the Gulf the latter is sufficiently the case that even for n=1 Poincaré modes are evanescent. Consequently away from either the mouth of the Gulf (where the Pacific effectively sets the cross Gulf variation of tidal elevation) or the closed end of the Gulf, the semidiurnal tide can consist only of a pair of oppositely travelling Kelvin waves.

Taylor (1921) considered the reflection of an incoming Kelvin wave from the closed end of a gulflike marginal sea. No pair of Kelvin waves can satisfy the condition of no normal flow at such a closed end; all the Poincaré modes are needed as well. But since they are evanescent, their influence decays exponentially away from the closed end so that some distance away from it only the Kelvin waves remain. If there is no dissipation, the reflected Kelvin wave has the same amplitude as the incoming Kelvin wave; their superposition displays amphidromic points spaced (π/k) apart along the centerline of thewaveguide. If there is energy loss in the vicinity of the closure, then the reflected Kelvin wave's amplitude is less than the amplitude of the incident Kelvin wave and the amphidromic points are shifted towards the 'outgoing' side. In the Gulf of California the outgoing side is Baja California. **Figure 1.1** (Hendershott and Speranza, 1971, Figures 2-5) shows tidal elevation for a sequence of problems with closure boundary condition $u_{normal}=\alpha\zeta$ in which the constant α varies from zero (no dissipation on reflection) to 0.56/sec (almost complete absorbtion of incident radiation). The shift of the amphidromic point towards the 'outgoing' side is very clear.

Now Miller (1966) estimated the total loss E_t of energy in the Gulf of California to be about 4×10^{17} ergs/sec. (For comparison, the energy lost to friction in the global tide - mainly in shallow seas such as the Bering Sea, the Sea of Okhtosk, the Timor Sea, the Patagonia Shelf - is about 2×10^{19} ergs/sec.) We thus expect a shift of the amphidromic point(s) in the Gulf of California.

A simple Kelvin wave fit (Hendershott and Speranza, 1971) to semidiurnal (M_2) tide gauge data at Guaymas, La Paz, Topolobampo and Mazatlan indeed shows a Baja-ward shift of the semidiurnal amphidrome (**Figure 1.2**, Hendershott and Speranza, 1971, Figure 10) implying corresponding appreciable energy dissipation north of the mid Gulf. Hendershott and Speranza (1971) estimated $E_t \approx 1.5\times10^{17}$ erg/sec for the M_2 tide from this fit.

Filloux's (1973) interpolation-without-dynamics of tide gauge observations clearly shows this shift of amphidrome (**Figure 1.3**; Filloux, 1973, Figure 2.) He can estimate sea level fluctuations ζ directly from his map, and cross-gulf-average tidal flow v from the draining of the tidal prism in northern gulf, and so can estimate directly the flux of energy $\langle\rho g\zeta vD\rangle$ x (Gulf Width) into the northern Gulf. He thus estimates $E_t \approx 4.35\times10^{16}$ erg/sec for the tide ($E_t \approx 4.85\times10^{16}$ erg/sec for all lunar tidal constituents). It is noteworthy that Filloux's cotidal map (Figure 1.3) puts the amphidrome a good deal further north than Hendershott and Speranza's map (Figure 1.2): this means that Hendershott and Speranza's map (a fit to Topolobamppo and La Paz) badly

overestimates the tide at Guaymas and hence probably overestimates the amplitude of the Kelvin wave on the continental coast of Mexico and the dissipation as well.

Stock (1976) constructed a numerical dynamical model of Gulf tides, and chose the spatial distribution of dissipation that best made the model match Filloux's collected observations in the sense of minimizing $\Sigma_{stations}$[model prediction - Filloux's observation]^2. He thus estimated both E_t and its along Gulf distribution. He found $E_t \approx (4.5 \text{ to } 5.0)\times 10^{16}$ erg/sec; the corresponding along-Gulf distributions of dissipation for various bottom stress laws are shown in **Figure 1.4** (Stock, 1976, Figures V-4 and V-6).

Tidal energy may be dissipated by various forms of friction, by conversion into internal waves and subsequent radiation, and finally in regions where strong velocity gradients occur in the interior of the fluid. (in the Gulf of California, such regions are the hydraulic jumps believed to occur as the tide floods southward or northward over the shallow sills in the narrow straits between the northern Gulf and Guaymas basin.) The foregoing estimates include contributions from all of these mechanisms. It is likely that much, indeed perhaps most, of the tidal energy dissipated in the Gulf is lost to bottom friction in the far northern Gulf or in the straits. I will not devote further attention to discussion of the physics and parameterization of this component of the dissipation because I believe Zimmerman will talk about it in his lectures. Instead I will concentrate on internal wave dissipation by radiation away from localized generation regions, and on dissipation in hydraulic jump regions.That disscussion follows immediately, but before reading it it may be helpful to look over the subsequent description of internal waves and hydraulic effects in the Gulf.

The most direct way to think about internal wave radiation of tidal energy lost to internal waves in localized generation regions is to look at the amount of energy that realistically large internal waves can cary away from generation regions, and ask whether or not it is is an appreciable fraction of all the energy dissipated. If the crests of tidally generated internal waves (possibly but not necessarily of tidal period) are a horizontal distance L long, then the radiated energy (ergs/sec) is LECg where E is the energy density (erg/cm^2) in a water column from sea surface to ocean floor and Cg is the group velocity of energy propagation. It turns out that the most energetic internal waves generated by tides in the gulf are not of tidal period, but instead are packets of much higher frequency waves (periods $\approx$ one hour). For these, the expressions for the period averaged potential energy density and group velocity are particularly simple:

$$PE = (1/2)\rho_0 \langle \int N^2\zeta^2\, dz \rangle, \qquad E = 2PE, \qquad Cg \approx \int N dz/(n\pi),$$

in which the vertical integrations are over the water column (of depth D), $\langle\rangle$ is the average over a wave period T e.g. $\langle\rangle = T^{-1}\int_0^T dt$, ζ is the vertical displacement of water parcels in the internal wave field, and and N(z) is the Brunt-Vaisala frequency (assumed greater than the wave frequency in the WKB approximation that led to the formula for Cg.) If the Brunt Vaisala frequency were a constant N_0, then for internal waves of maximum vertical displacement N_0,

$$LECg \approx [(L/4)\rho_0 N_0^2 \zeta_0^2 D\,][N_0 D/n\pi].$$

If we take L=50km, N_0=2cph, D=300m and ζ_0 = 50m, we get LECg = 3.7×10^{16} erg/sec. As will be seen below, each packet consists of a few crests and troughs and hence takes a few hours to pass by a particular location. The average amount over a tidal period of energy radiated is thus not just LECg but rather [(duration of packet / tidal period) LECg] ; it is thus the order of about 10^{16} erg/sec, the order of 20% of the estimates of Filloux (1973) and of Stock (1976). On the basis of a somewhat more detailed description of the wave packets as viewed from SEASAT SAR images,

Fu and Holt (1984) estimated a upper bound of $5x10^{15}$ erg/sec for the loss of tidal energy to travelling internal waves in the gulf.

Tidal energy may be lost at the generation region as well as by subbsequent radiation awayn from the generation region.The discussion below indicates that the generation regions are places where supercritical flow with hydraulic jumps and travelling bores may occur. Dissipation in internal hydraulic jumps in a two layer flow is discussed by Baines (1984). Since however the two layer approximation is not nearly as good over the gulf sills as it is, for example, in the Straits of Gibraltar (e.g. Armi and Farmer, 1988 and papers cited there), a simple discussion along the lines of, e.g. Lamb (1932) is all that is available in order to roughly estimate energy loss in hydraulic jumps or bores occuring during the tidal cycle. Imagine therefore a near bottom layer of dense fluid of thickness h and flow speed u under a deeper and quiescent upper layer. If there is a transition in layer depth, both mass flux $Q=uh$ and momentum flux $M=u^2h+g'h^2/2$ (per unit mass and unit width of jump) must be the same on either side of the transition but the energy flux $E=uh(u^2/2 + g'h)$ will decrease (where g' is the vertical acceleration g of gravity multiplied by the relative density difference $\Delta\rho/\rho$ between moving and quiescent layers, e.g. the reduced gravity). Since, from these,

$$M=Q^2/h+g'h^2/2\,, \qquad E=Q[Q^2/(2h^2) + g'h],$$

we have

$$\Delta M = Q^2(1/h_2 - 1/h_1) + (g'/2)\,(h_2^2 - h_1^2) = 0,$$

$$\Delta E = (Q/2)[\, Q^2(1/h_2^2 \; - \; 1/h_1^2) + 2g'(h_2 - h_1)\,]$$

so that finally

$$\Delta E = (g'Q/4)\,\Delta h^3/(h_1h_2),\;\; \Delta h = (h_1 - h_2)$$

This multiplied by the cross-sill with L of the jump or bore and by the density ρ of the moving fluid gives the energy loss per second as fluid flows through the jump. If we take $g=1000$ cm/sec^2, $\Delta\rho/\rho = .001$, $h = 400$ m, $u = 1.0$ m/sec, and $L = 10$ km (for all jumps over all sills) we get

$$\Delta E_{total} = (\rho g'Lh^2u/4)\,[\Delta h^3/(hh_1h_2)] = 4x10^{16}\,[\Delta h^3/(hh_1h_2)] \text{ erg/sec.}$$

The uncertainties in this estimate are large; it must be adjusted downward to account for the facts that hydraulic conditions vary widely over a tidal cycle and that flow at neaps may be subcritical. The factor $[\Delta h^3/(hh_1h_2)]$ is probably substantially less than one; the following discussion summarizes what little is known about the sizes of parameters needed to make this estimate. Taken at face value, it suggests that gulf-wide dissipation in jumps and bores is probably only a fraction of the energy radiated in internal wave packets, although in the vicinity of the sills it may be very important.

2. Internal Wave Packets and Hydraulic Phenomena in the Gulf of California

In August, 1974 a CALCOFI Cruise in the Gulf of California recorded evidence of high amplitude (order 50 m) undulatory displacements of isotherms over San Lorenzo sill. **Figure 2.1** shows the location of hydrographic stations along a section passing from the north end of Ballenas Channel southward over San Lorenzo sill into Guaymas basin together with the depths of selected isotherms along the section. The wavelike pattern in isotherms over San Lorenzo sill cannot be taken too literally, as time variation of the actual pattern is probably seriously aliased into it; nonetheless it is clear that large vertical excursions of fluid parcels occur near this sill. Similarly great vertical excursions have since been documented over San Esteban sill, over the sill at the north end of Ballenas Canal, and over San Lorenzo spur.

Patterns strongly suggesting internal wave packets propagating away from San Lorenzo sill and away from the three other locations just noted are prominent in the synthetic aperture radar (SAR) images recorded by SEASAT in July-October of 1978 (Fu and Holt, 1984). It is not known with certainty what feature of the sea surface outlines the internal wave field in these images; most likely the radar responds to the effect of internal wave orbital currents on small (centimeter scale) surface waves. **Figure 2.2** (Fu and Holt, 1984, Figure 2) is a typical spring tide image; packets were clearly visible at spring tides, and barely detectable at neaps. **Figure 2.3** shows the locations of the leading crests of the most prominent groups visible in a number of images. They appear to eminate from the four locations noted above, although close study of the images shows a wealth of less prominent detail associated either with secondary reflections of waves from these packets or else with waves generated at other sites.

In January 1990, Badan et al (1991) made simultaneous five hour long vertical profiles of temperature (by yoyoing a CTD) and of horizontal and vertical velocities (with a shipboard acoustic doppler logger current profiler made by RDInstruments of San Diego, CA). **Figure 2.4** (Badan et al, 1991, Figure 4) shows the results. Since the wave period is so short (about one hour) the earth's rotation may be neglected. Taking y to be the direction of wave propagation (with velocity v in the y direction), the waves satisfy

$$v_t = -\Pi_y, \qquad N^2 w = -\Pi_{zt}, \qquad v_y + w_z = 0$$

where w is vertical velocity in the upward (z) direction (z=0 at the surface), N is the Brunt-Vaisala frequency, and $\Pi = p/\rho o$ where p is the pressure. If the Vaisala frequency is constant (N_o), then first mode solutions are

$$v = v_o(y-ct)\cos(\pi z/D), \qquad \Pi = \Pi_o(y-ct)\cos(\pi z/D),$$

$$w = w_o(y-ct)\sin(\pi z/D), \qquad \zeta = \zeta_o(y-ct)\sin(\pi z/D,$$

in which ζ is the vertical displacement, $w = \zeta_t$, the propagation speed is $c=N_oD/\pi$ and the functions w_o, ζ_o are related to v_o by

$$w_o = v_{ot}\ (D/c\pi), \qquad \zeta_o = v_o\ (D/c\pi) = v_o/N_o.$$

(Note that, inconveniently, the choice of z=0 at the sea surface makes w_o, $\zeta_o < 0$ correspond to upward vertical velocity or displacement, respectively.) These relationships are clearly visible in Figure 2.4.

At this station the Brunt-Vaisala frequency N is about 2 cph and the depth is about 315 m so that $c=ND/\pi$ = 0.3 m/sec. Since the wave period is about an hour, the wavelength is about 1100 m. The ratio between vertical and horizontal velocities for periodic motions (period T) is w_o/v_o = $2\pi/NT = 2\pi/(4\pi$ rph x 1 hour) =1/2. The vertical displacement of isotherms is about 70 m.

Over the sills, the water column at spring tides is instantaneously frequently statically unstable over many tens of meters. Thus for example the vertical profiles of temperature, salinity and density over San Esteban sill as the spring tide floods southward that are shown in **Figure 2.5** show unstable stratification over the lower half of the water column. At such times, the profiles evolve so rapidly that the down and up parts of the cast appear unrelated.

Figure 2.6 (Paden,1991, Fig 21 plus individual temperature profiles) shows the results of an XBT transect southward over this sill as the tide flooded southward. The extreme vertical excursions (over 200 m!) of fluid parcels implied by the isotherm displacements are especially noteworthy, as is the location just downstream of the sill of the most unstably stratified temperature profile.

The extreme vertical excursions of isotherms imply that very cold water is brought to the surface in these regions. This will be documented in more detail in the discussion of the large scale circulation, where it will be suggested that this is an important mechanism in the overall heating of the northern Gulf by the atmosphere. The sea surface in these regions around spring tides shows patches of water tens to hundreds of meters across into which short waves cannot propagate, suggesting violent upwelling in their centers. A aircraft IR sensor map of sea surface temperature over San Esteban sill when the tide is flooding northward shows a cold patch about a kilometer in diameter on the north side of the sill.

In January of 1990, Badan et al (1991) returned to this site with the Acoustic Doppler Current Profiler and took some sections over the sill as the tide flooded southward. **Figure 2.7** (Badan et al, 1991, Fig. 3) shows one such transect together with isotherms from an electrical BT. Because the tide turned about the time the ship passed over the sill, appreciable time variation of the flow is aliased into this transect. Nonetheless, the important point for this discussion is that the measured tidal velocities are greater than the local speed of first mode internal waves over most of the transect; the flow is supercritical. The spring tidal cycle in these regions will thus be marked by the occurence and dissolution of internal hydraulic jumps as the current increases and decreases; these are probably closely connected with the radiation of the internal wave packets whose occurence has been documented above.

3. Coastally Trapped Waves in the Gulf of California.

Christensen et al (1983) and Enfield and Allen (1983) have found poleward propagating nondispersive events in sea level along the Pacific coast of Mexico in summer-fall over the frequency range 0.02 to 0.37 cpd. They seem to originate in the alongshore polward movement of tropical storms as far as 20°N and thereafter propagate as free events into the Gulf at least as far as Guaymas. **Figure 3.1** (Enfield and Allen, 1983, Fig. 2) shows a number of such events in 1971, and **Figure 3.2** (Enfield and Allen, 1983, Fig. 5) shows details of two such events together with the tracks of the storms believed to have produced them.

More recently Merrifield and Winant (1989) have again observed such events in the Gulf, but in alongshore current and bottom pressure as well as in sea level. **Figure 3.3** (Merrifield and Winant, 1989, Figure 14) shows such events in sealevel and bottom pressure from Salina Cruz (about 16°S and 1000 km away from the mouth of the Gulf along the Pacific coast of Mexico) to

San Francisquito, about 100 km north of Guaymas inside the Gulf). Within the Gulf, events appear to propagate at roughly 200-250 kpd.

Extensive measurements along the Guaymas-Santa Rosalia line give a good idea of the spatial structure of pressure fluctuations in the water column as these events pass Guaymas towards the northern Gulf. Bottom pressure measurements and density measurements in the overlying water column allow reconstruction of p(x,z.t) during events such as the energetic one from 8-15 July of 1984. **Figure 3.4** (Merrifield and Winant, 1989, Figure 15) shows (panel a) offshore decay of the bottom pressure signal away from Guaymas and (panel c) decay with depth of pressure signal in offshore column 200 m deep. **Figure 3.5** (Merrifield and Winant, 1989, Figure 16) shows the spatial distribution of the pressure signal associated with the domonant EOF of pressure along this transect; the offshore decay scale is about 50 km and the vertical decay scale is about 150 m. As will be seen below, this signal is uncorrelated with Guaymas winds or with winds over the Gulf (they turn out to be very similar).

The flow associated with this pressure signal is strongly geostrophic in the cross-shelf direction. Figure 5 (Merrifield and Winant, 1989, Figure 21) compares the observed along-shelf flow and the geostrophic flow (computed from the foregoing estimate of the pressure signal) near Guaymas and near Santa Rosalia. Observations of the along-shelf flow v and of $(f\rho_0)^{-1}dp/dx$ are significantly correlated at both stations with correlation coefficients of 0.47 at Guaymas and 0.41 at Santa Rosalia; the regression coefficients are 0.71 and 1.09 respectively. It is clear to the eye that the correlation is substantially higher during the most energetic event (July 8-15, 1984).

In the along-shore direction the local acceleration is strongly correlated with the alonshore pressure gradient but not at all with local winds, indicating wave propagation towards the northern Gulf. Thus **Figure 3.6** (Merrifield and Winant, 1989, Figure 23) shows that v_t and $\rho_0^{-1}dp/dy$ at Guaymas and Santa Rosalia correspond well during events. **Table 3.1** (Merrifield and Winant, 1989, Table 5) shows that v_t and $\rho_0^{-1}dp/dy$ are well correlated at both stations; especially along the Guaymas shelf break $\rho_0^{-1}dp/dy$ accounts for over 40% of the variance in v_t. The correlation is greatest at a lag of about 15 hours in part because the estimate of $\rho_0^{-1}dp/dy$ uses instruments at Guaymas and Isla Tiburon, and hence is centered about 50 km north of Guaymas (this would produce a lag of about 50km/250kpd ≈ 5 hours, why the observed lag is appreciably larger is not known). **Table 3.1** also shows that along-shore wind stress τ^y accounts for virtually none of the variance in along-shore acceleration, as would be expected for remotely generated signals.

Finally, in the most energetic event of 8-15 July 1984 **Figure 3.7** (Merrifield and Winant, 1989, Figure 24) shows that the vertical displacement of isotherms is a mirror image of sea level displacement with about a 60 m fall of isotherms in the upper 130 m corresponding to a 20 cm rise in sea level. As sea level rises, fluctuations in the flow are northward; all these signals are in the sense expected for a poleward propagating Kelvin wave.

It is natural to ask whether such propagating disturbances can be reflected in the far northern Gulf and return southward along the coast of Baja California. In fact, **Figure 3.8** (Merrifield and Winant, 1989, Figure 25) shows that in both 1983 and 1984, near coastal pressure or adjusted (inverse barometer removed) sealevel signals at Guaymas consistently reappear 7 to 9 days later in temperature fluctuations at 70-100 m depth just offshore of Santa Rosalia. **Table 3.2** (Merrifield and Winant, 1989, Table 2) shows similar correlation between offshore temperatures at Guaymas and Santa Rosalia, but no similar lagged correlation appears in corresponding currents.

Bibliography, Waves in the Gulf of California

Armi, L. and D. Farmer (1988). The flow of Mediterranean Water Through the Strait of Gibraltar. Progress in Oceanography, 21, pp. 1-105.

Baines, P. G. (1984). A unified description of two-layer flow over topography. Jour. Fluid Mech., 146, pp. 127-167.

Christensen, N., Jr., R. de la Paz, and G. Gutierrez (1983). A study of sub-inertial waves off the west coast of Mexico. Deep Sea Res., 30, p 835-850.

Enfield, D. and J.S. Allen (1983). The generation and propagation of sea level variability along the Pacific coast of Mexico. Jour. Phys. Oceanog., 13, pp 1012-1033.

Filloux, J. H. (1973). Tidal Patterns and Energy Balance in the Gulf of California. Nature, 243, pp. 217-221.

Fu, L-L and B. Holt (1984). Internal Waves in the Gulf of California: Observations From a Spaceborne radar. Jour. Geophys. Res., 89, pp. 2053-2060.

Hendershott, M. C. and A. Speranza (1971). Co-oscillating tides in long, narrow bays; the Taylor problem revisited. Deep Sea Res., 18, pp. 959-980.

Lamb, H. (1932). Hydrodynamics. Dover Publications, New York, sixth edition, 738 pp.

Merrifield, M. A. and C. D. Winant (1989). Shelf Circulation in the Gulf of California: A Description of the Variability. Jour. Geophys. Res., 94, pp. 18133-18160.

Miller, G. R. (1966). The flux of tidal energy out of the deep ocean. Jour. Geophys. Res., 71,. pp. 2485-2489.

Stock, G. G. (1976). Modelling of Tides and Tidal Dissipation in the Gulf of California. PhD Thesis, University of California in San Diego, 133 pp.

Taylor, G. I. (1921) Tidal oscillations in gulfs and rectangular basins. Proc. Lond. Math. Soc., 20, pp 148-181.

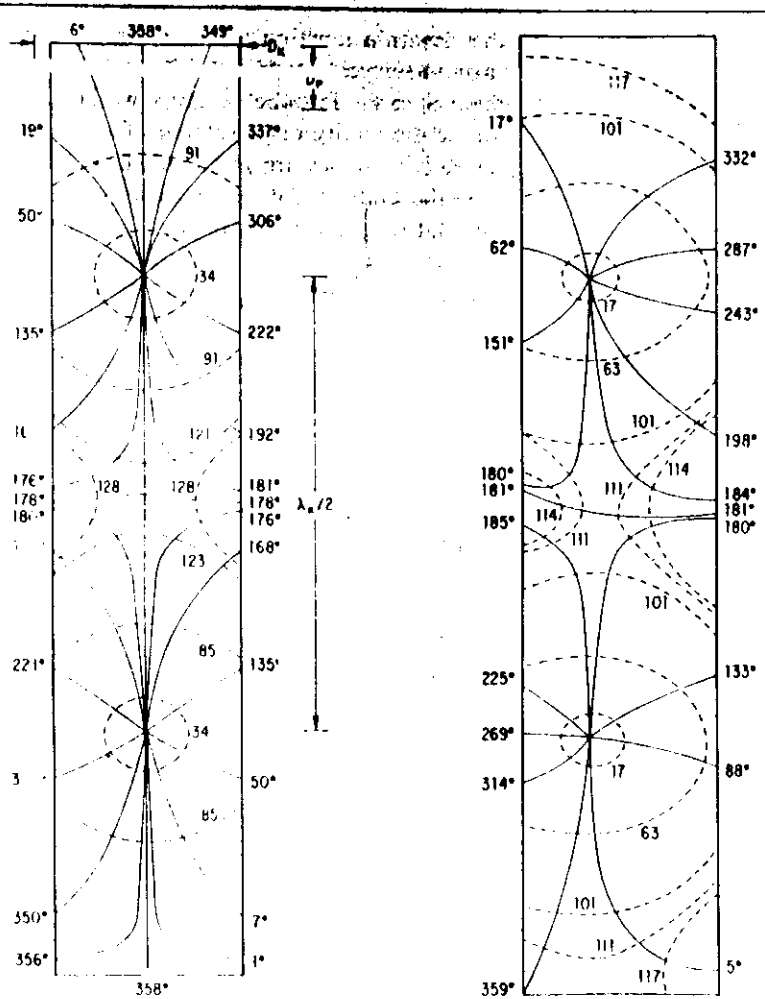

Fig. 2. $\alpha = 0$.

Fig. 3. $\alpha = 0{\cdot}056$ sec^{-1}.

Figs. 2–5. Complete ($\alpha = 0$) or partial ($\alpha = 0{\cdot}056$ sec^{-1}, $\alpha = 0{\cdot}28$ sec^{-1}, $\alpha = 0{\cdot}56$ sec^{-1}) reflection an M_2 Kelvin wave in a rectangular bay of 200 km width, 50 m depth at a latitude of 45°. Phases in degrees, amplitudes in arbitrary units.

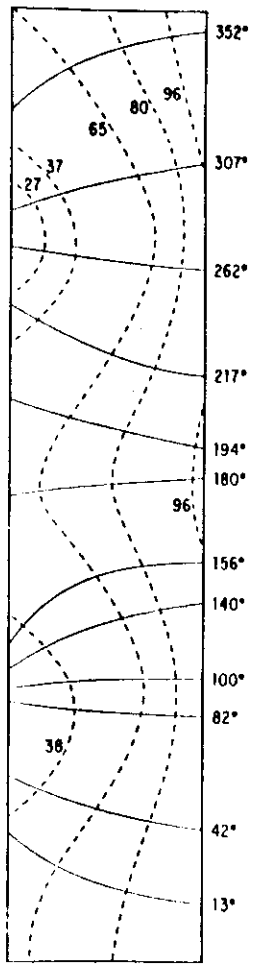

Fig. 4. $\alpha = 0{\cdot}28$ sec^{-1}.

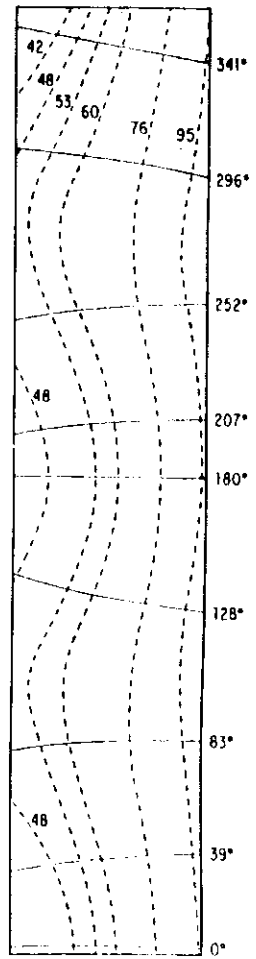

Fig. 5. $\alpha = 0{\cdot}56$ sec^{-1}.

Miller 4×10^{17} e/s

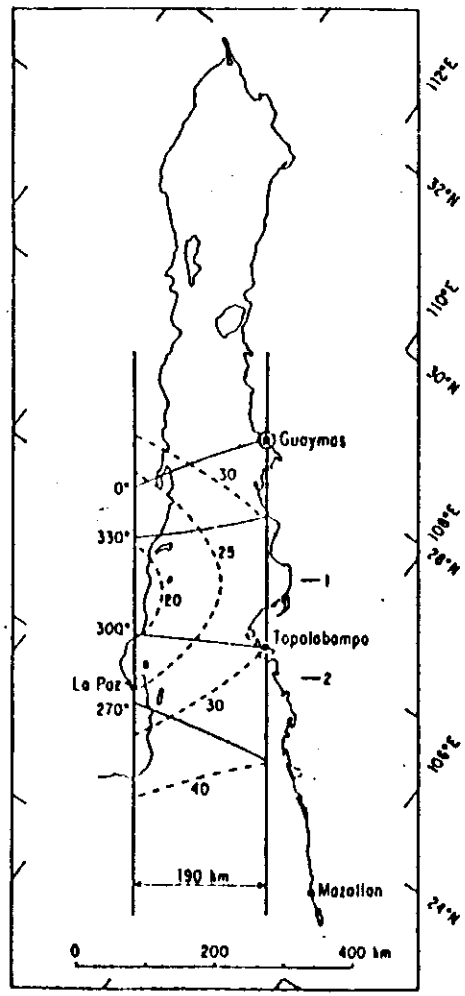

2.13×10^{17} e/s

MCH + AS

(1.7)

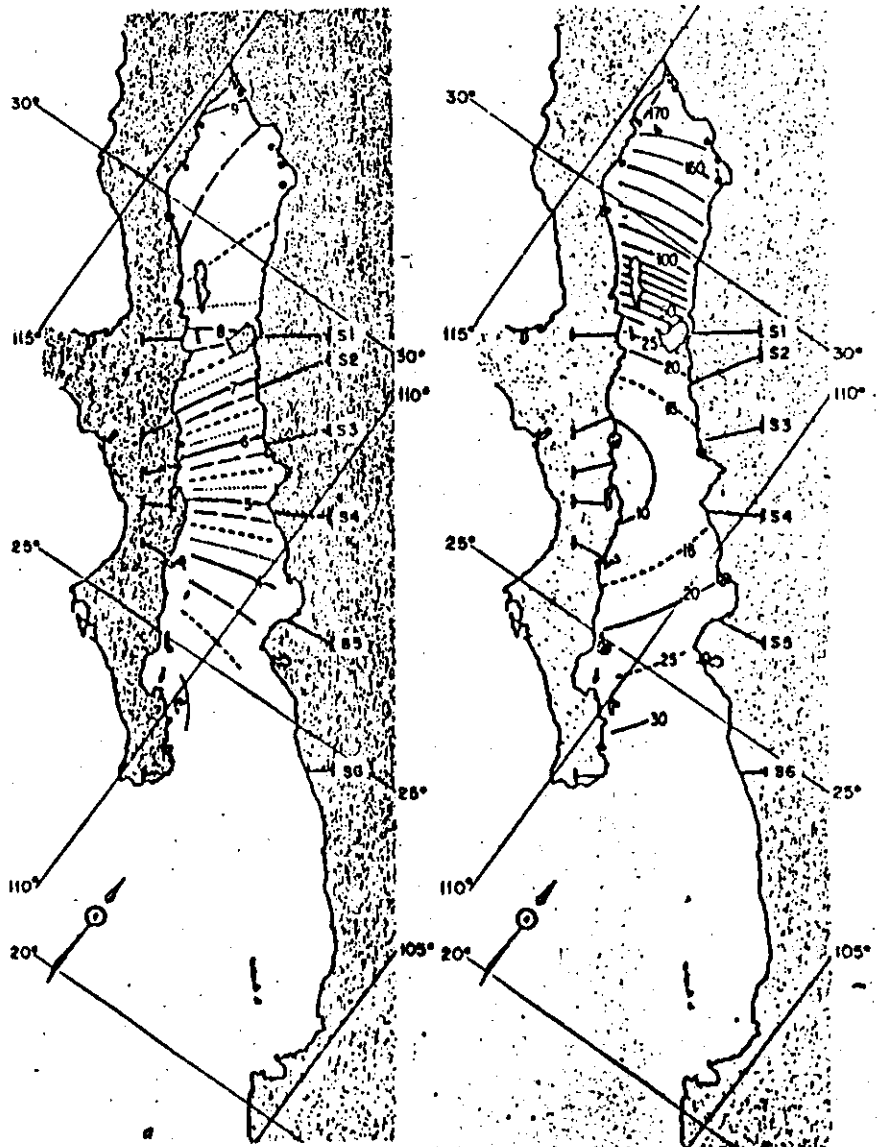

Filloux 4.70×10^{16} e/s

(1.7)

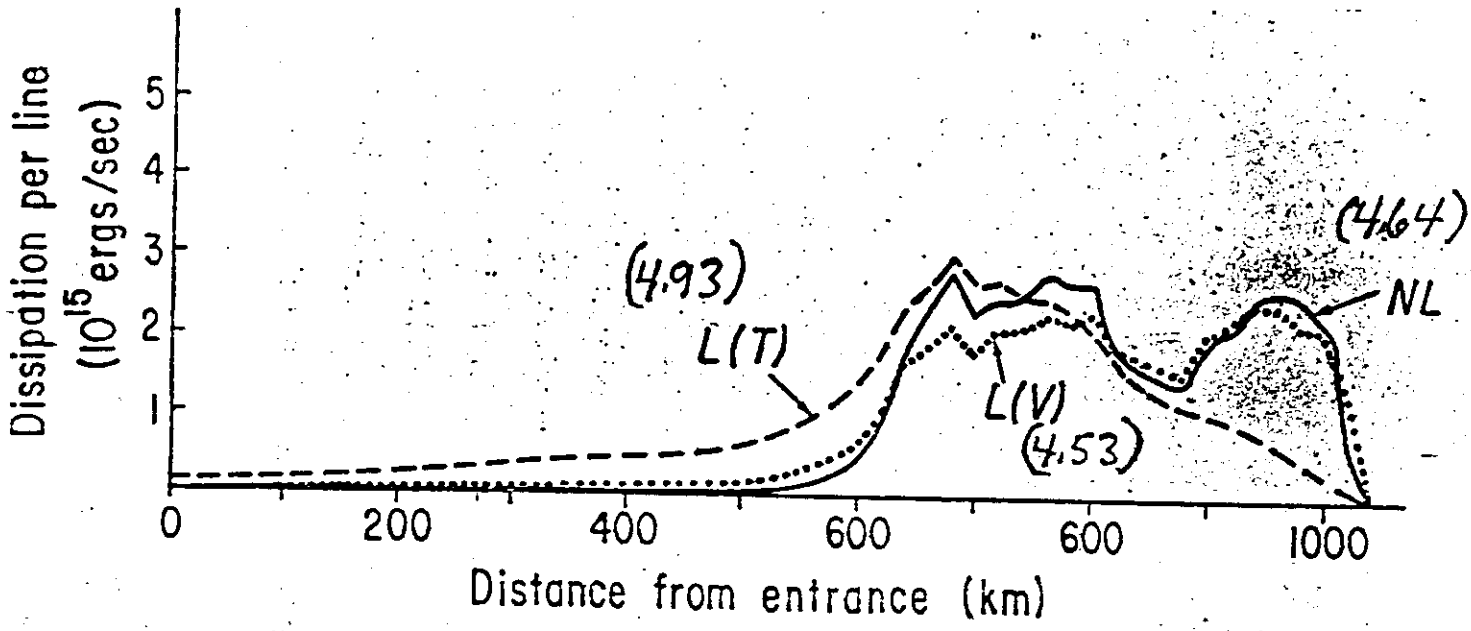

FIGURE V-4. Variation along the Gulf of the average dissipation per 20 km wide transversal band given by M2 optimized models with various bottom stress laws.

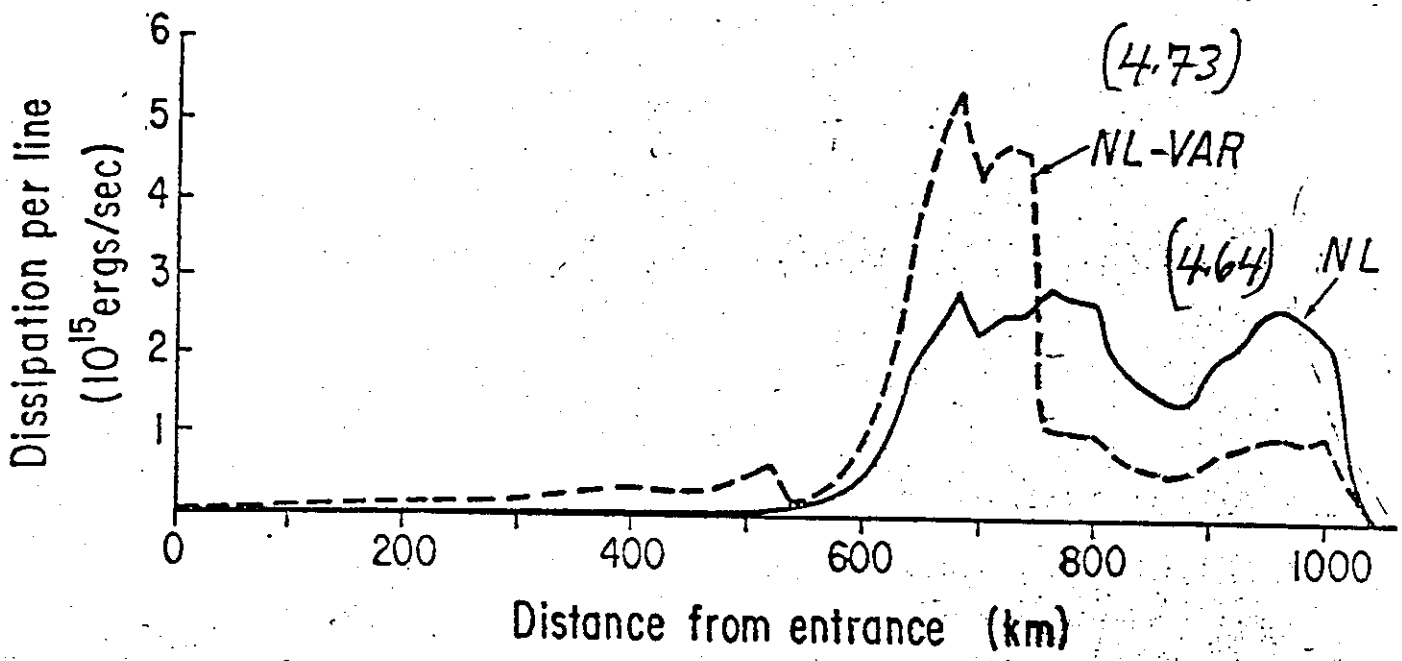

FIGURE V-6. Dissipation distribution of optimized M2 model with variable quadratic friction coefficient (NL-VAR) in comparison to constant coefficient model (NL).

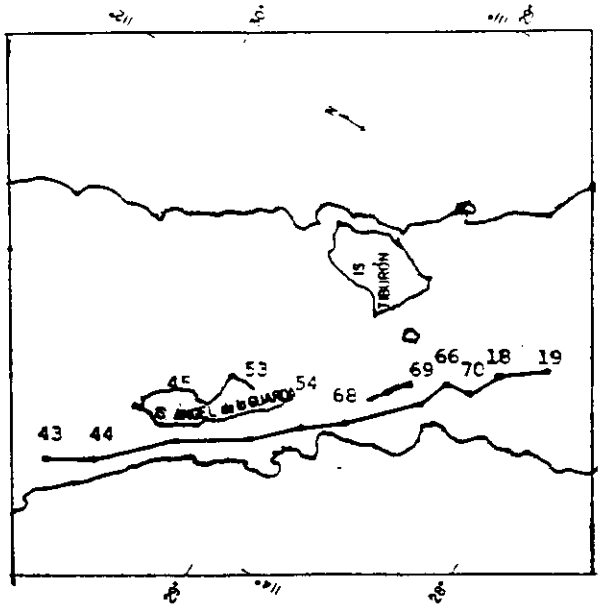
IS
TIBURON
45
53
54
68
69
66
70
18
19
43
44

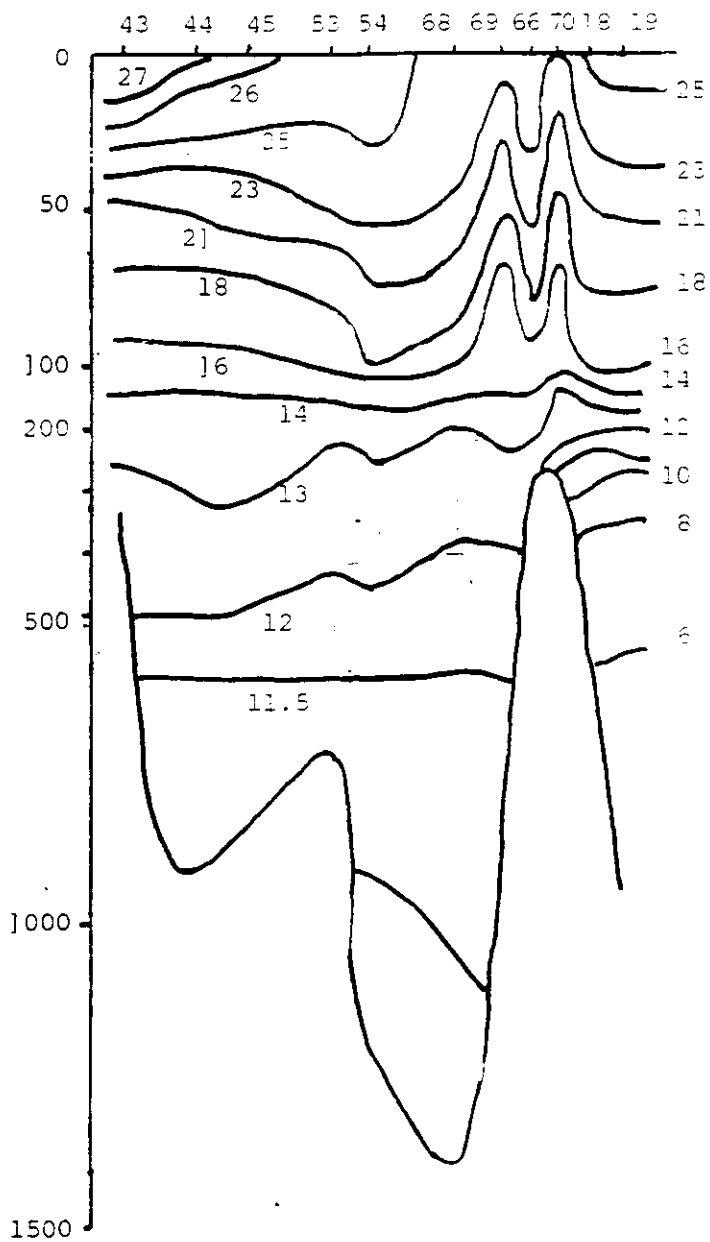
43
44
45
53
54
68
69
66
70
18
19
0
50
100
200
500
1000
1500
27
26
25
23
21
18
16
14
13
12
11.5
25
23
21
18
16
14
12
10
8
6

2.1

Fig. 2. SAR image taken on [illegible] 1985 (image 2) of the area identified by the rectangle shown in Figure 1.

Fig. 3. As Figure 2 except that the image was taken on [illegible] 1985 (image 3).

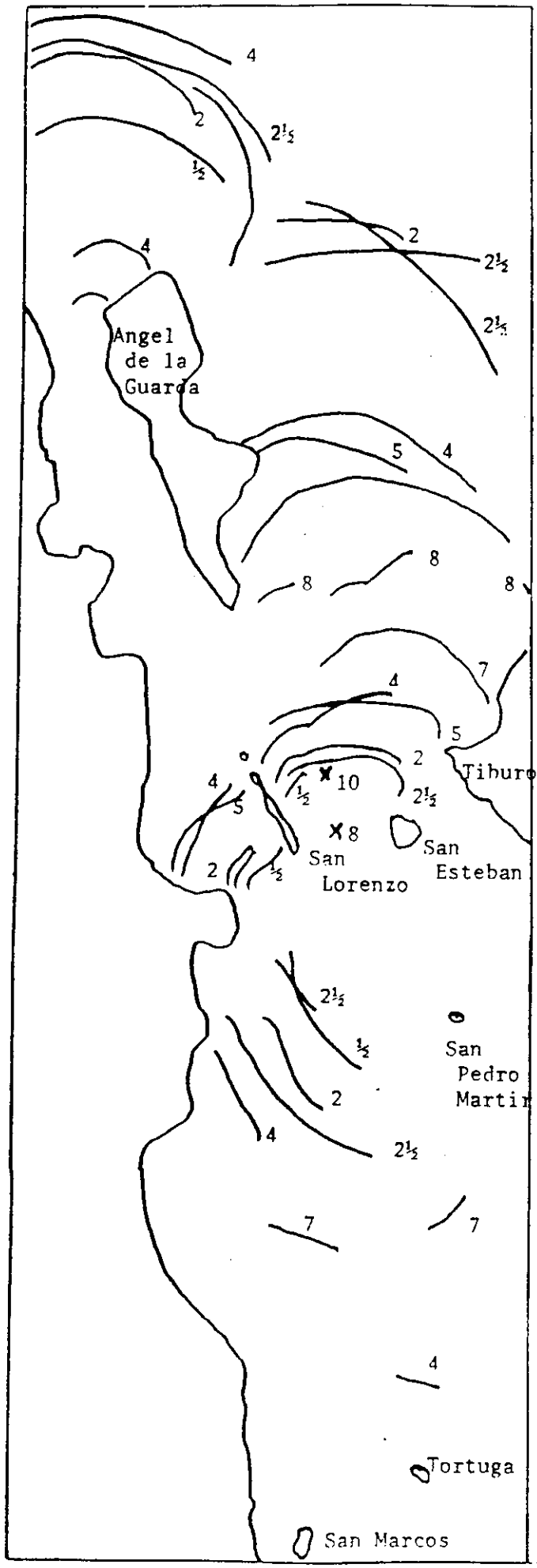
4
2
2½
½
2
2½
2½
4
Angel
de la
Guarda
5
4
8
8
8
7
4
5
2
10
Tiburon
4
5
½
2½
8
San
Lorenzo
San
Esteban
2
½
2½
½
San
Pedro
Martir
2
4
2½
7
7
4
Tortuga
San Marcos

Locations of leading crests of internal wave groups visible on SEASAT SAR images labeled in hours (rounded to nearest) after foregoing low tide at Puerto Penasco. Islands and coastline sketched from Rev 1355 and Rev 1140. It is not known whether occasional apparent failure of crests to progress uniformly is due to missing initial crest, to changes in projection from one image to another (images were not registered to common grid), or to time variable currents.

Rev	Date	Time (GMT)	(MST)	Low Tide (MST)	Lag
1226	20 Sept	17:31	10:31	9:53	0:38 (½)
1183	17 Sept	17:15	10:15	8:06	2:09 (2)
1441	5 Sept	18:33	11:33	9:06	2:27 (2½)
1140	14 Sept	17:04	10:04	6:07	3:58 (4)
1355	29 Sept	18:11	11:11	6:23	4:48 (5)
193	10 July	12:20	05:20	22:26#	6:54 (7)
387	24 July	02:13*	19:13	10:56	8:17 (8)

preceeding day
* following day

Stations Y8 and Y9, occupied 8 and 10 hours after foregoing low tide, are marked by x's between Isla San Esteban and Isla San Lorenzo.

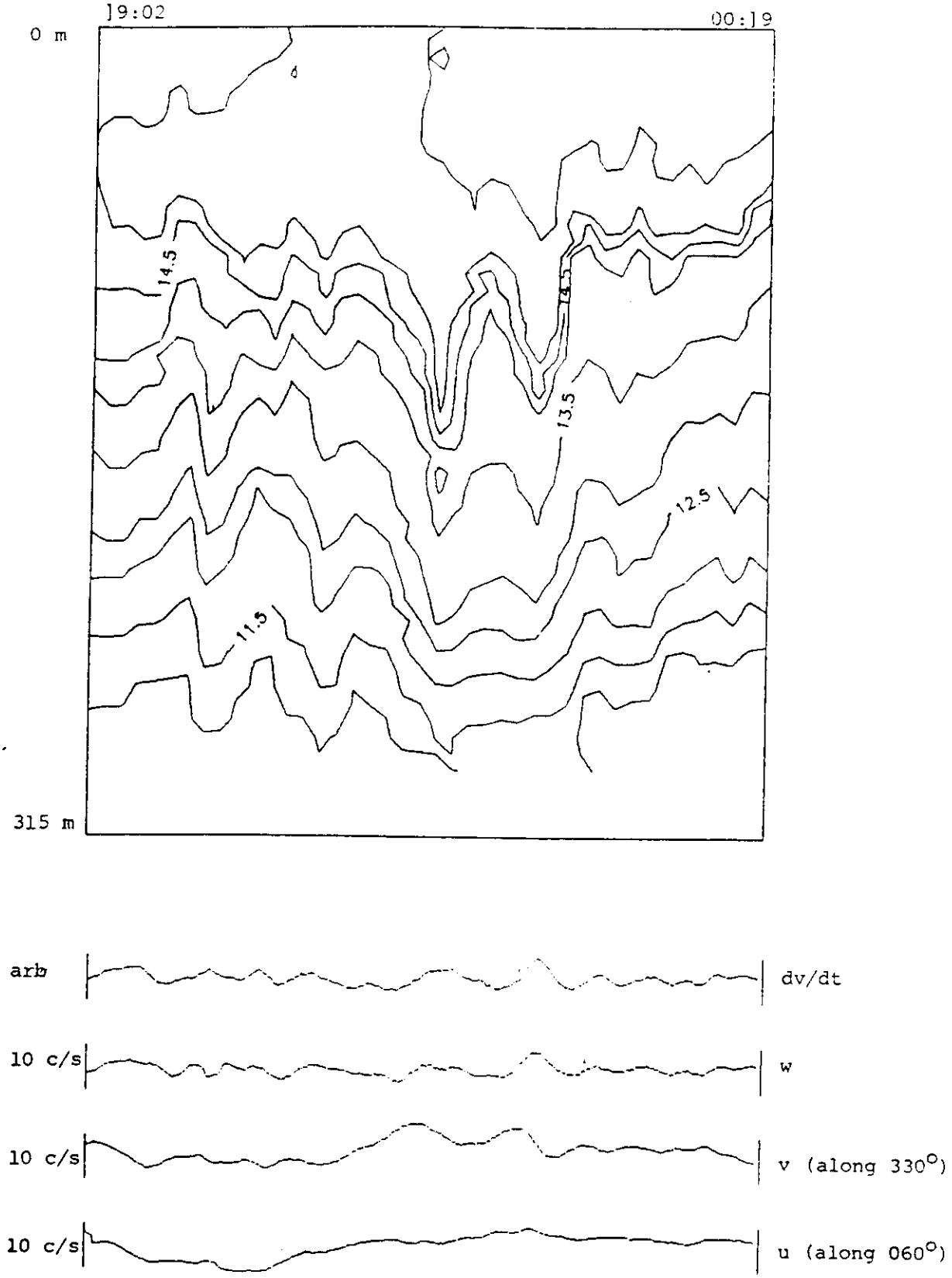
19:02
00:19
0 m
315 m
14.5
14.5
13.5
12.5
11.5
arb
dv/dt
10 c/s
w
10 c/s
v (along 330°)
10 c/s
u (along 060°)

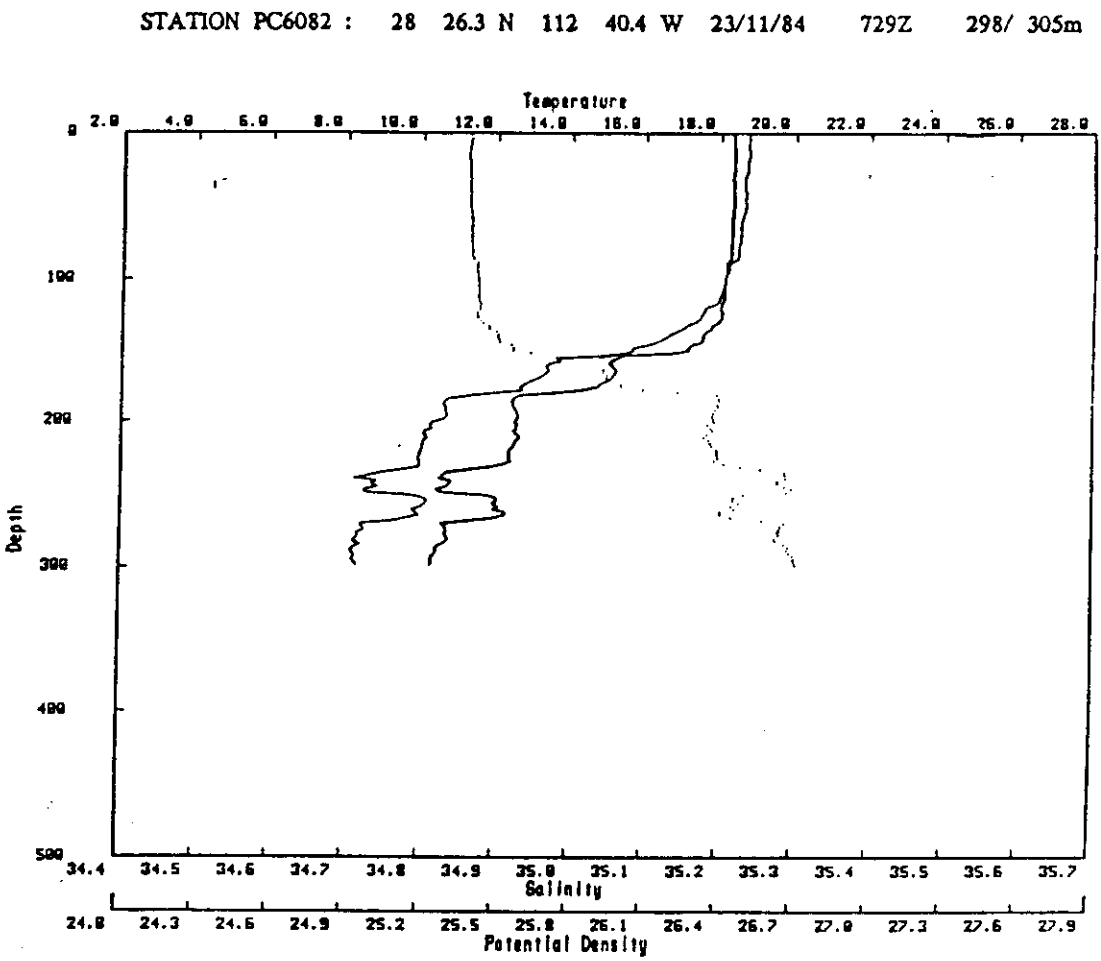

Figure 2.4.3a: Temperature (°C, dark line), salinity (ppm, light line), and potential density (standard units, dotted line) profiles at station 82 of Pichicuco 6, near San Esteban sill.

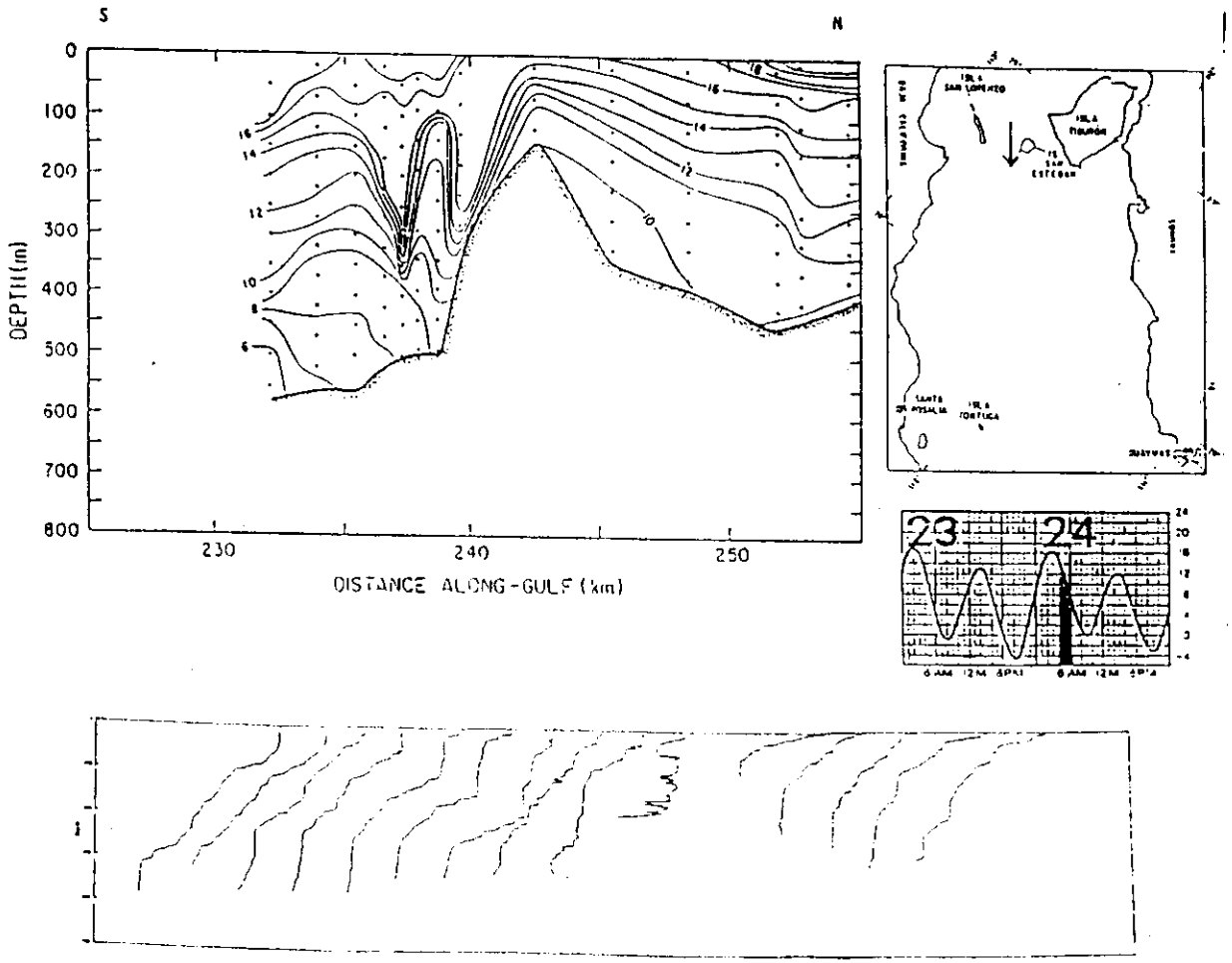

Figure 2.4.4: XBT temperature transect SE1 southward across San Esteban sill at spring tides, on the 24th of November 1984, as the tide floods southward, during cruise Pichicuco 6. Inset map shows transect path; inset tide gauge record at Puerto Peñasco also shows time of transect. (a) isotherms (°C); after Paden, 1990. (b) Individual temperature profiles (temperature in °C versus depth in meters) offset along the temperature axis in rough correspondence with geographical position as indicated in (a) above. Ticks on temperature scale are every 2 °C; depth scale is 0 to 750 m.

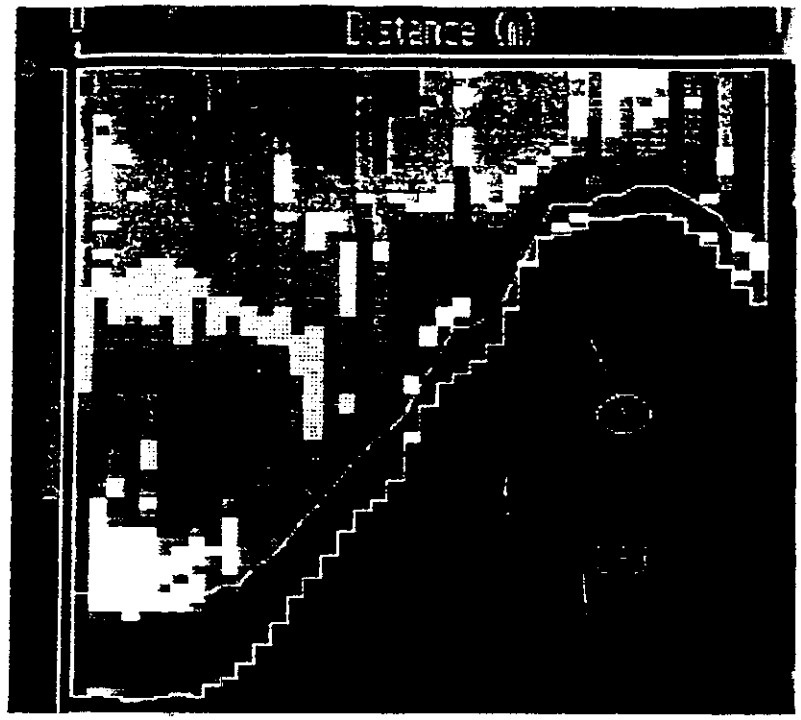
Distance (m)

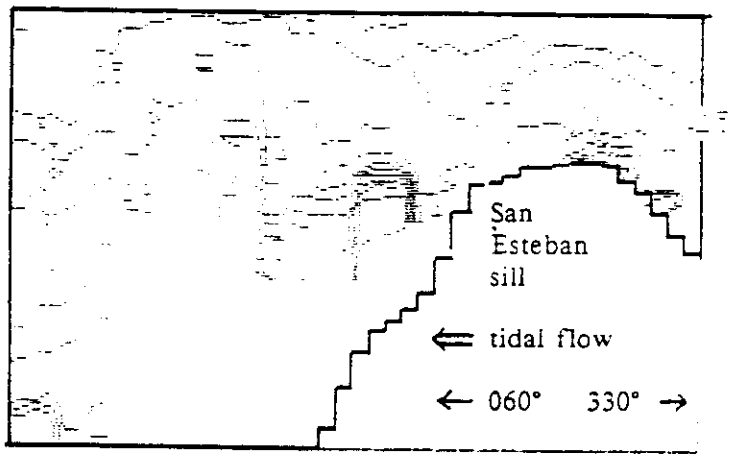
San
Esteban
sill
⇐ tidal flow
← 060° 330° →

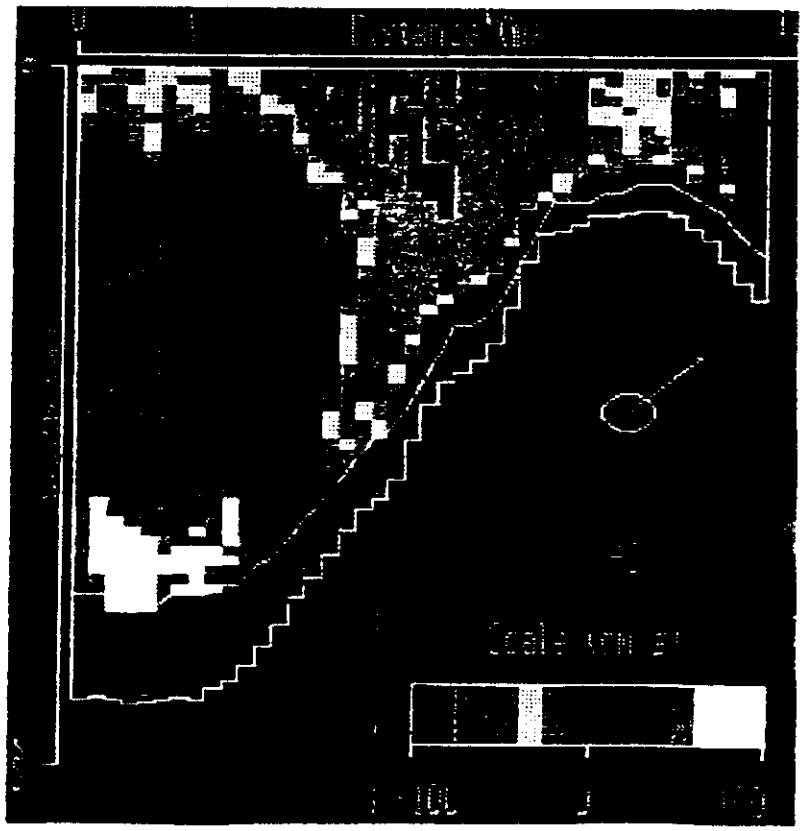
Distance (m)

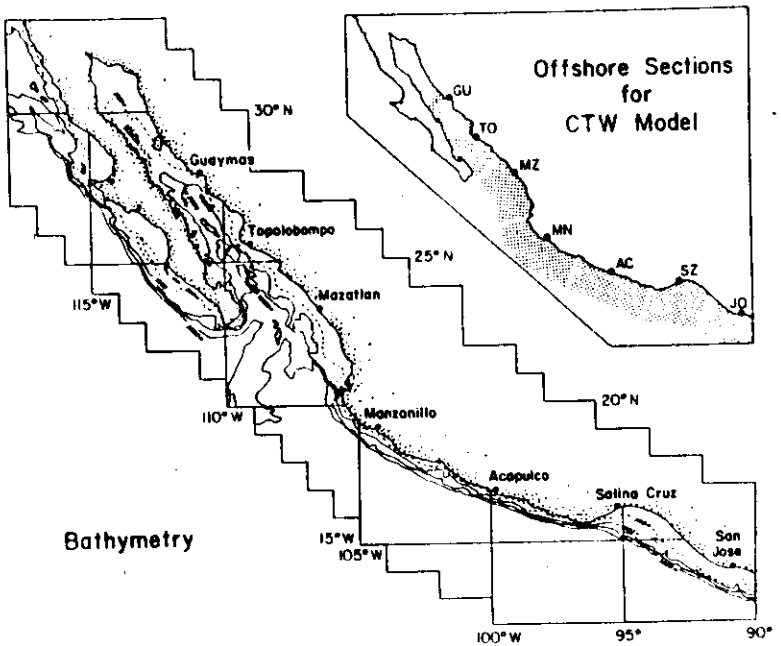

FIG. 1. Locations of sea level stations and bathymetry chart for the Pacific coast of Mexico, with isobaths shown for depths of 200 m (dashed) and 1000, 2000 and 3000 m (solid). Inset at upper right is a map showing the coastal sections for which the coastal-trapped wave model of Brink (1982) was run (Section 6).

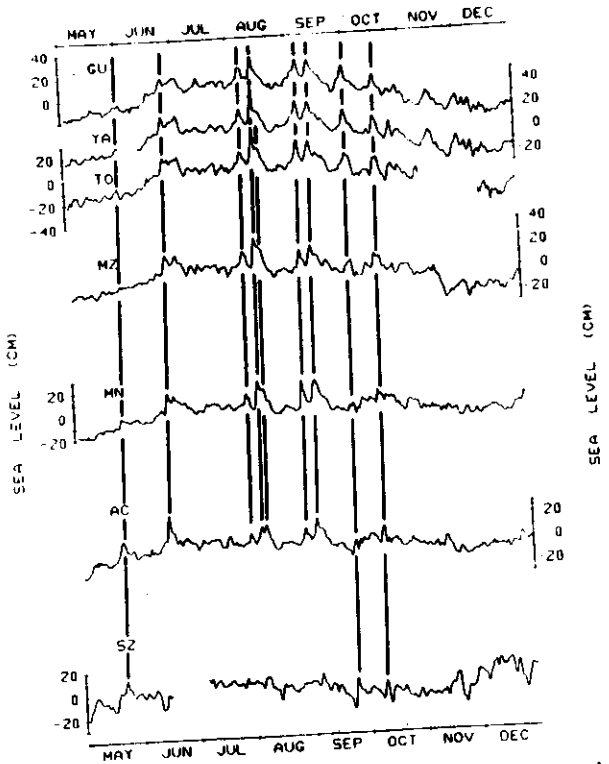

FIG. 2. Low-pass filtered sea level heights at tide stations on the mainland coast of Mexico, in 1971 (annual harmonic not removed). Time series are vertically spaced in proportion to the station separations. Location abbreviations are defined in Table 1, except YA (Yavaros, 27°N). Straight lines indicate propagating events associated with tropical storms.

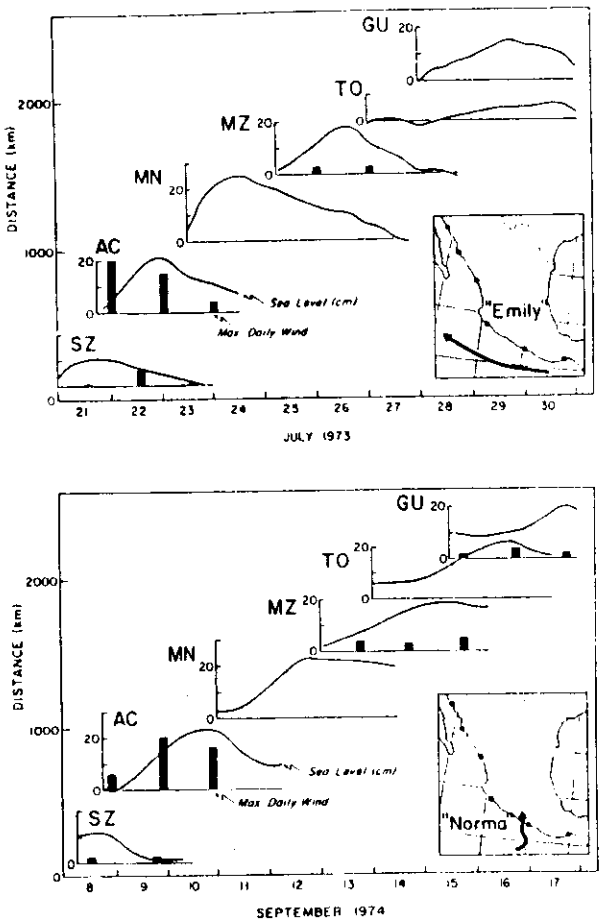

FIG. 5. Case history diagrams for two propagating sea level events. A time–distance plot of sea level height (solid line, cm) and maximum daily winds (vertical bars, m s^{-1}) during the passage of an event is shown for each tide station, with its origin at the appropriate time and position. The inset maps show the hurricane tracks associated with the sea level events. No wind observations are available for the stations at which wind bars are not plotted.

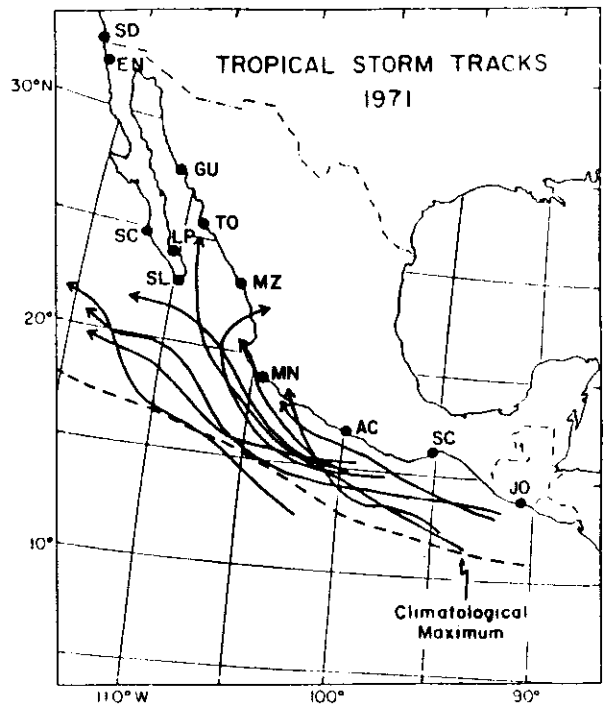

FIG. 3. Tracks of tropical storm centers that passed within 500 km of the Mexican coast in 1971 (solid lines). Dashed line indicates the locus of maximum occurrence of tropical storm centers (Thompson, *et al.*, 1981).

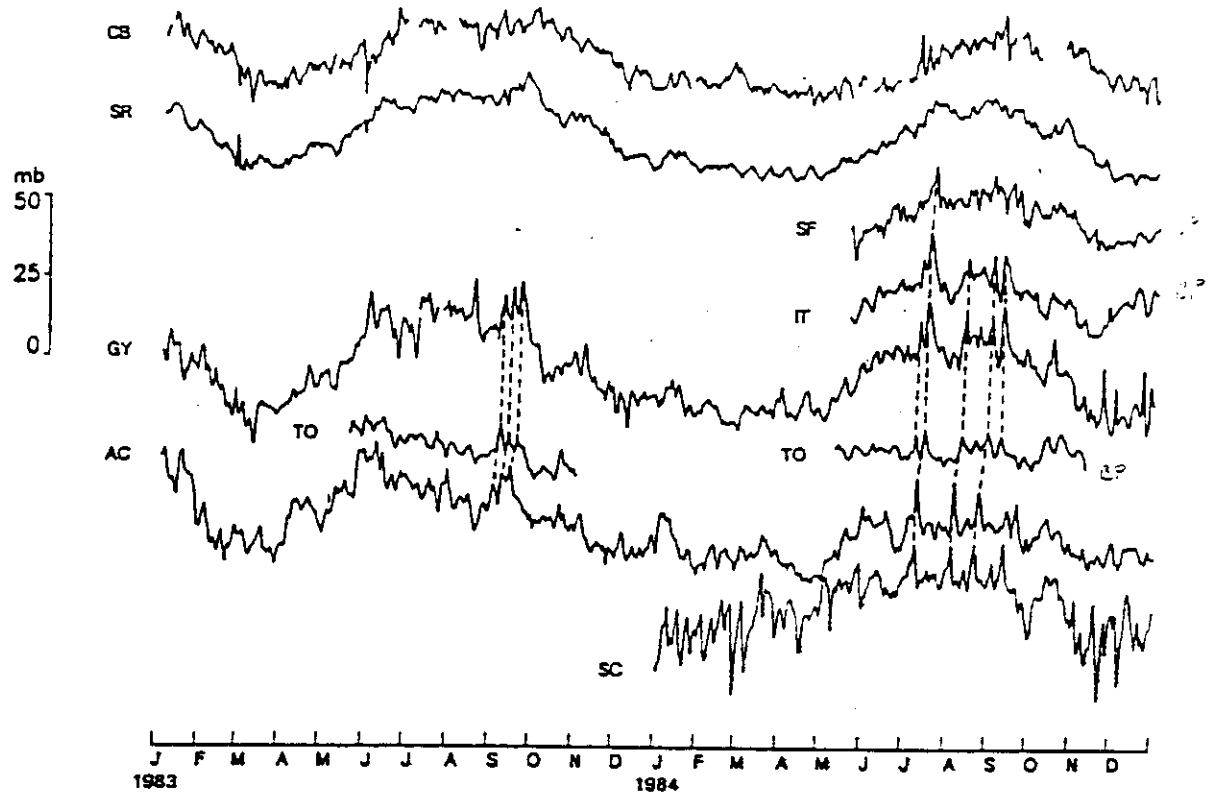

Fig. 14. Sea level and pressure along the Mexican Pacific coast and in the Gulf of California during 1983–1984. Energetic propagating events are connected between stations. Guaymas and Santa Rosalia sea level have been adjusted for the inverse barometer effect. Bottom pressure time series are shown from Topolobampo (P1), San Francisquito (P7), and Isla Tiburon (P10). Stations are CB, Cabo San Lucas; SR, Santa Rosalia; SF, San Francisquito; IT, Isla Tiburon; GY, Guaymas; TO, Topolobampo; AC, Acapulco; SC, Salina Cruz.

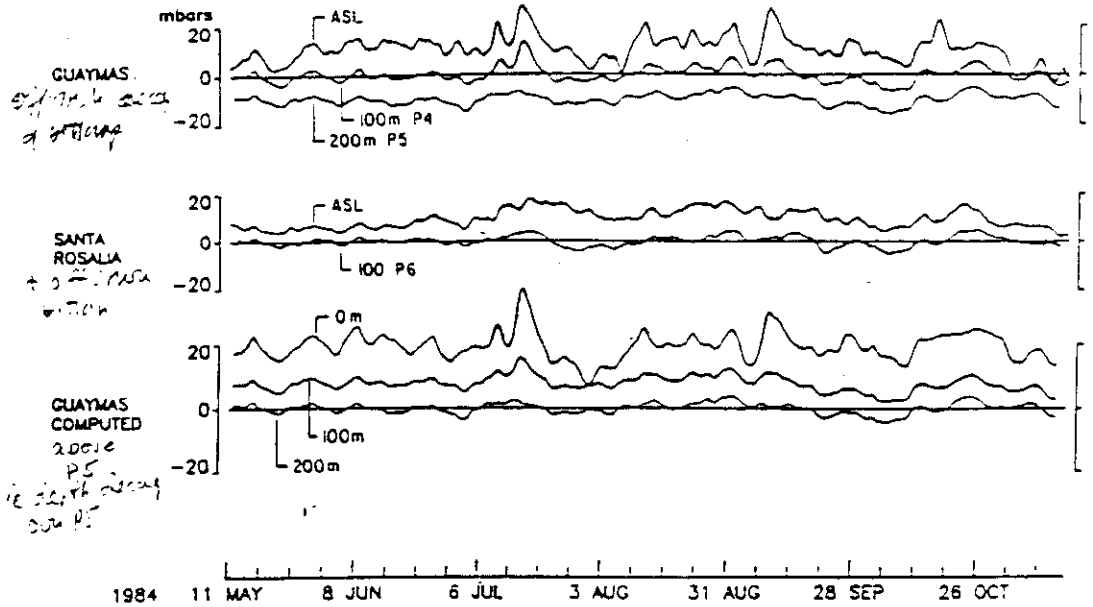

Fig. 15. Adjusted sea level and bottom pressure at 100 m (P4) and 200 m (P5) at Guaymas, adjusted sea level and 90-m bottom pressure (P6) at Santa Rosalia, and Guaymas computed pressure at 0 m and 100 m above the 200-m (P5) sensor, using equation (2).

3.4

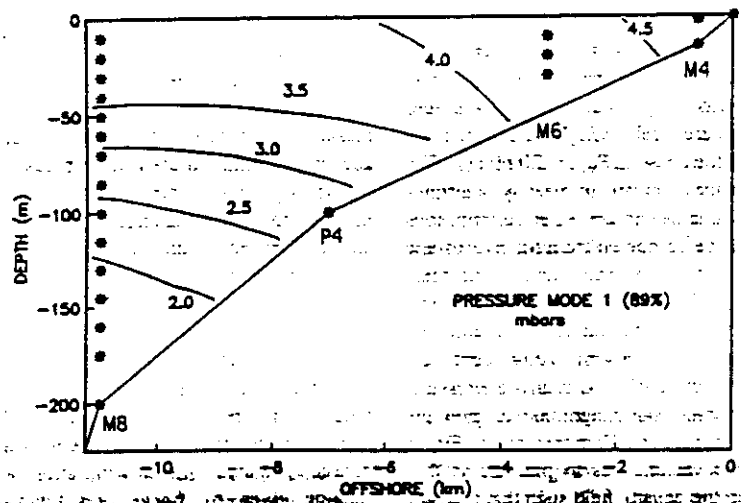

Fig. 16. The mode 1 spatial EOF of low-frequency pressure fluctuations on the Guaymas shelf. Asterisks indicate locations of pressure observations used in forming the EOF, including adjusted sea level at the coast, and computed pressure using temperature observations. Surface pressure at M6 is constructed from a weighted average of adjusted sea level at the coast and surface pressure at M8.

3.5

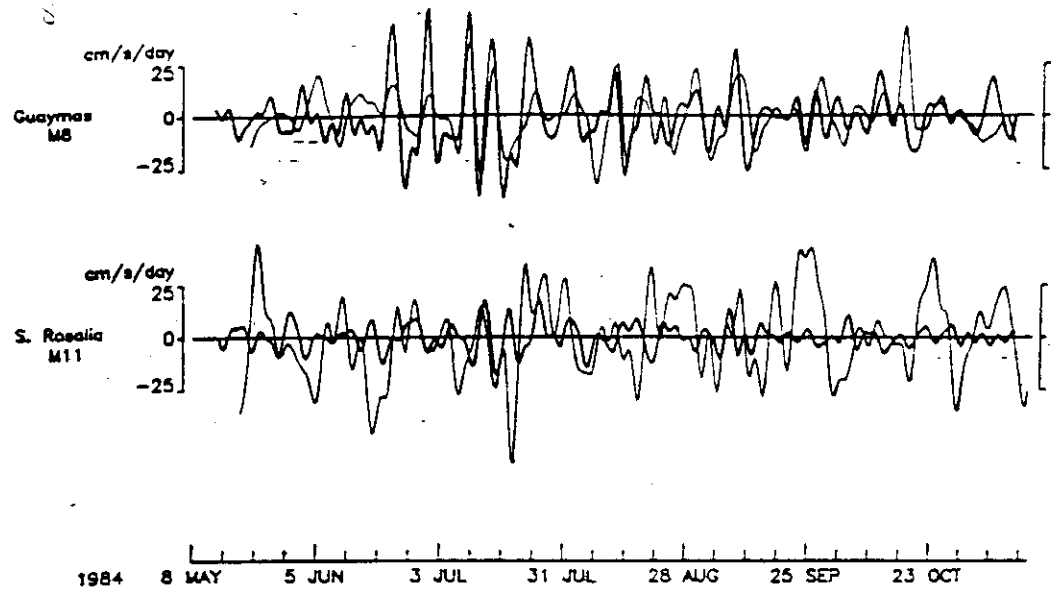

Fig. 23. The time derivative of alongshelf currents (dark lines) at Guaymas ($M8_{10m}$) and Santa Rosalia ($M11_{10m}$) versus the alongshelf pressure gradient (light). The pressure gradient is obtained from the near-surface pressure difference between Guaymas and Isla Tiburon (P10) on the mainland shelf, and Santa Rosalia and San Francisquito (P7) on the Baja California shelf.

3.6

TABLE 5. Multivariate Analysis of the Alongshelf Pressure Gradient (dP/dy) and Along-Gulf Wind Stress Regressed on dV/dt at Various Moorings From Equation (6)

	Hindcast Skill (x100)	dP/dy β_1	Lag, hours	Variance,%	τ^y β_2	Lag, hours	Variance,%
dV/dt							
$M4_5$	11.2*	-0.05 ± 0.06	0	11.3	0.02 ± 0.03	0	1.0
$M6_{20}$	14.9*	-0.27 ± 0.27	-37	15.5	-0.04 ± 0.15	0	0.1
$M8_{20}$	41.6*	-0.82 ± 0.61	-15	33.0	0.51 ± 0.33	0	3.7
$M9_{10}$	9.1	-0.11 ± 0.09	0	4.4	0.06 ± 0.06	0	4.9
$M11_{70}$	7.7*	-0.09 ± 0.05	32	4.3	0.06 ± 0.06	0	3.5
$M11_{10}$	2.7*	-0.05 ± 0.03	33	2.6	0.01 ± 0.05	0	0.1
$M11_{30}$	6.5*	0.00 ± 0.03	33	2.3	-0.06 ± 0.05	0	5.5
$M11_{70}$							

Hindcast skill is the amount of variance explained in the regression; the variance listed represents that explained by each input. Mooring subscripts indicate VMCM depths.
* Above 95% significance level.

$$V_t = \beta_1 P_y + \beta_2 \tau^y$$

Table 3.1

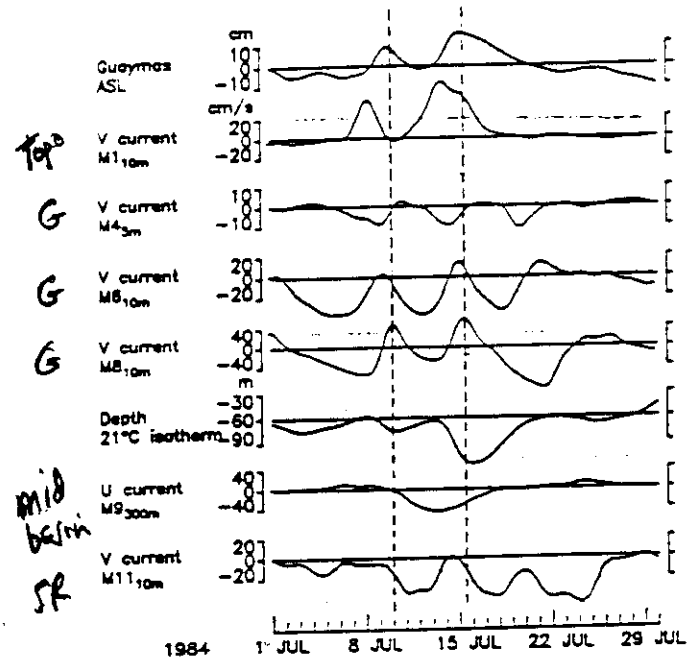

Fig. 24. Current and temperature observations in the Gulf of California during the most energetic propagating event of 1984 as seen in adjusted sea level at Guaymas.

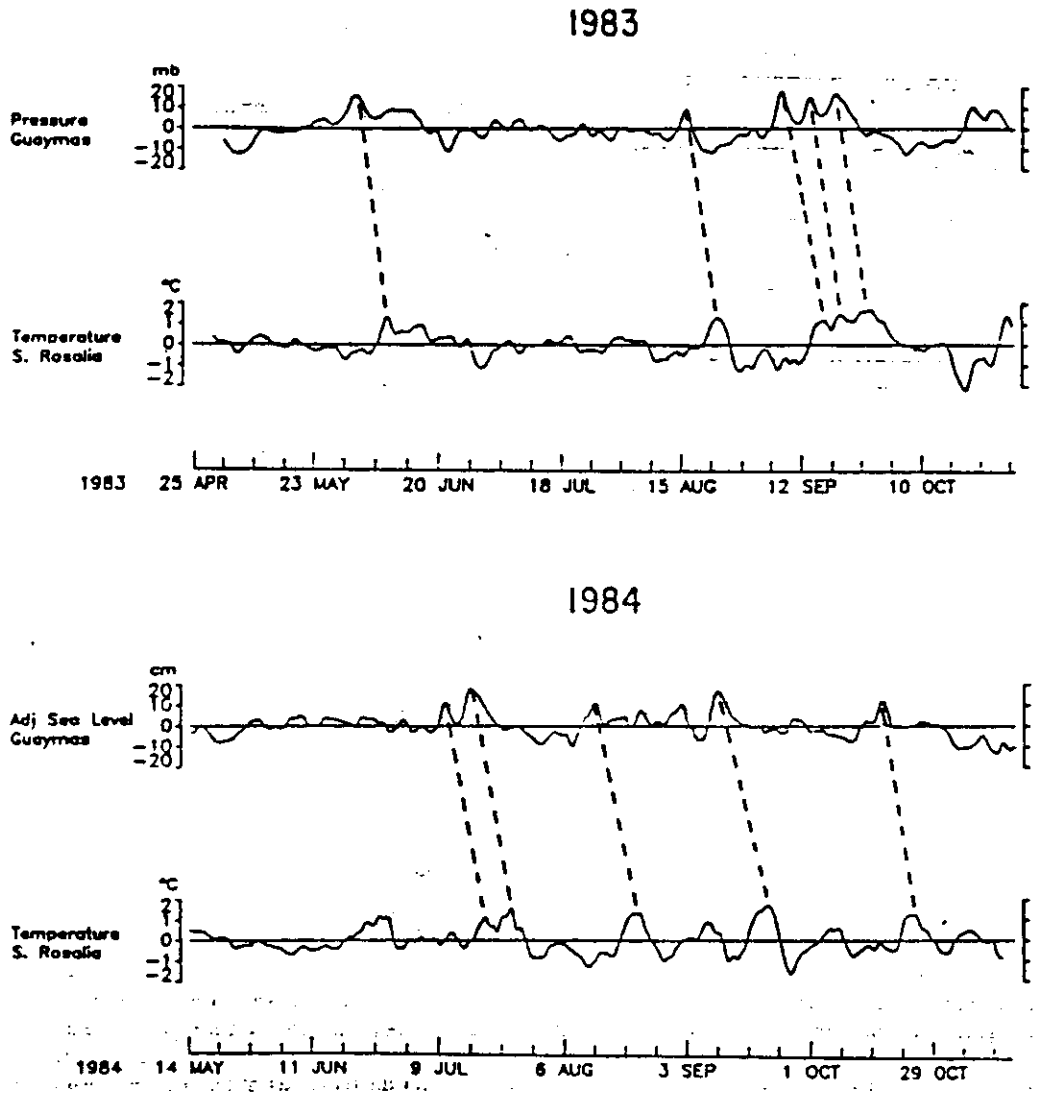

Fig. 25. Comparison of shallow bottom pressure and adjusted sea level at Guaymas with temperature at Santa Rosalia for the summers of 1983 and 1984. Events which appear to correspond in both records are connected.

3.8

TABLE 2. Correlations for Low Frequency Temperature Records During the Summer–Fall Deployments of 1983 and 1984

Instrument Location	Correlation	Maximum Correlation	Lag, days
	1983 Deployments		
Topolobampo–Guaymas			
$M1_{10}$ - $M7_{10}$	0.78*		0.0
$M1_{70}$ - $M7_{75}$	0.52*	0.62*	1.38
$M1_{100}$ - $M7_{75}$	0.54*	0.73*	- 1.63
Topolobampo–Santa Rosalia			
$M1_{10}$ - $M11_{10}$	0.66*		0.0
$M1_{70}$ - $M11_{65}$	0.04	0.67*	8.42
$M1_{100}$ - $M11_{86}$	-0.02	0.69*	9.29
Guaymas–Santa Rosalia			
$M7_{10}$ - $M11_{10}$	0.50*	0.56*	7.13
$M7_{75}$ - $M11_{65}$	0.14	0.62*	7.50
$M7_{75}$ - $M11_{86}$	0.08	0.71*	7.33
	1984 Deployments		
Topolobampo–Guaymas			
$M1_{10}$ - $M8_{10}$	0.16		0.0
$M1_{70}$ - $M8_{70}$	0.45*	0.64*	1.79
$M1_{100}$ - $M7_{100}$	0.47*	0.67*	1.58
$M1_{100}$ - $M8_{100}$	0.45*	0.64*	1.79
Topolobampo–Santa Rosalia			
$M1_{70}$ - $M11_{70}$	0.07	0.39*	9.42
$M1_{100}$ - $M11_{90}$	0.03	0.46*	9.21
Guaymas–Basin			
$M8_{50}$ - $M9_{50}$	-0.16		0.0
$M8_{100}$ - $M9_{100}$	-0.21		0.0
Guaymas–Santa Rosalia			
$M8_{10}$ - $M11_{10}$	-0.08		0.0
$M8_{30}$ - $M11_{30}$	-0.21		0.0
$M8_{70}$ - $M11_{70}$	-0.03	0.55*	8.96
$M7_{100}$ - $M11_{90}$	0.03	0.55*	8.46
Basin–Santa Rosalia			
$M9_{50}$ - $M11_{30}$	0.09		0.0
$M9_{100}$ - $M11_{100}$	0.36		0.0

Instrument location is represented by mooring number followed by depth of sensor beneath the surface. Maximum correlations, if different than zero-lag correlation, and time lag for maximum correlation are also listed. A positive lag means that temperature at the first sensor leads the second.
* Above 95% significance level

Table 3.2